

Single-pulse coherent anti-Stokes Raman scattering microscopy employing an octave spanning pulse

Keisuke Isobe¹, Akira Suda¹, Masahiro Tanaka², Hiroshi Hashimoto²,
Fumihiko Kannari², Hiroyuki Kawano³, Hideaki Mizuno³, Atsushi Miyawaki³, and
Katsumi Midorikawa¹

¹Keisuke Isobe Laser Technology Laboratory, RIKEN, 2-1 Hirosawa, Wako, Saitama 351-0198, Japan

²Department of Electronics and Electrical Engineering, Keio University, 3-14-1 Hiyoshi, Kohoku-ku, Yokohama 223-8522, Japan

³Laboratory for Cell Function Dynamics, RIKEN Brain Science Institute, 2-1 Hirosawa, Wako, Saitama 351-0198, Japan

kisobe@riken.jp

Abstract: We demonstrate two complementary types of microscopy using an identical setup for single-pulse coherent anti-Stokes Raman scattering (CARS) imaging, which employs an ultrabroadband laser pulse with a spectral bandwidth of 4800 cm^{-1} and enables the suppression of nonresonant CARS signals. One is a novel type of microscopy that uses spectral phase modulation for the selective excitation of a single Raman mode. The selective excitation is achieved by the modulated pulse focusing its difference-frequency spectrum into a narrow spectral region. Another type is Fourier-transform CARS (FT-CARS) microspectroscopy based on the measurement of the CARS spectrum obtained from the Fourier-transform of the interferometric autocorrelation (IAC) signal. Vibrational spectral imaging of chemical and biological samples is demonstrated using the two types of microscopy.

©2009 Optical Society of America

OCIS codes: (180.4315) Nonlinear microscopy; (170.5660) Raman spectroscopy; (320.5540) Pulse shaping; (300.6300) Spectroscopy, Fourier transforms.

References and links

1. M. D. Duncan, J. Reintjes, and T. J. Manuccia, "Scanning coherent anti-Stokes Raman microscope," *Opt. Lett.* **7**(8), 350–352 (1982).
2. A. Zumbusch, G. R. Holtom, and X. S. Xie, "Three-dimensional vibrational imaging by coherent anti-Stokes Raman scattering," *Phys. Rev. Lett.* **82**(20), 4142–4145 (1999).
3. E. O. Potma, D. J. Jones, J. X. Cheng, X. S. Xie, and J. Ye, "High-sensitivity coherent anti-Stokes Raman scattering microscopy with two tightly synchronized picosecond lasers," *Opt. Lett.* **27**(13), 1168–1170 (2002).
4. J. Cheng, A. Volkmer, L. D. Book, and X. S. Xie, "An Epi-Detected Coherent Anti-Stokes Raman Scattering (E-CARS) Microscope with High Spectral Resolution and High Sensitivity," *J. Phys. Chem. B* **105**(7), 1277–1280 (2001).
5. A. Volkmer, J. Cheng, and X. S. Xie, "Vibrational Imaging with High Sensitivity via Epi-detected Coherent Anti-Stokes Raman Scattering Microscopy," *Phys. Rev. Lett.* **87**, 023901/1–4 (2001).
6. E. O. Potma, C. L. Evans, and X. S. Xie, "Heterodyne coherent anti-Stokes Raman scattering (CARS) imaging," *Opt. Lett.* **31**(2), 241–243 (2006).
7. C. L. Evans, E. O. Potma, and X. S. Xie, "Coherent anti-stokes raman scattering spectral interferometry: determination of the real and imaginary components of nonlinear susceptibility $\chi(3)$ for vibrational microscopy," *Opt. Lett.* **29**(24), 2923–2925 (2004).
8. J. L. Oudar, R. W. Smith, and Y. R. Shen, "Polarization-sensitive coherent anti-Stokes Raman spectroscopy," *Appl. Phys. Lett.* **34**(11), 758–760 (1979).
9. J. X. Cheng, L. D. Book, and X. S. Xie, "Polarization coherent anti-Stokes Raman scattering microscopy," *Opt. Lett.* **26**(17), 1341–1343 (2001).
10. A. Volkmer, L. D. Book, and X. S. Xie, "Time-resolved coherent anti-Stokes Raman scattering microscopy: Imaging based on Raman free induction decay," *Appl. Phys. Lett.* **80**(9), 1505–1507 (2002).
11. N. Dudovich, D. Oron, and Y. Silberberg, "Single-pulse coherently controlled nonlinear Raman spectroscopy and microscopy," *Nature* **418**(6897), 512–514 (2002).

12. D. Oron, N. Dudovich, and Y. Silberberg, "Single-Pulse Phase-Contrast Nonlinear Raman Spectroscopy," *Phys. Rev. Lett.* **89**, 273001/1–4 (2002).
13. N. Dudovich, D. Oron, and Y. Silberberg, "Single-pulse coherent anti-Stokes Raman spectroscopy in the fingerprint spectral region," *J. Chem. Phys.* **118**(20), 9208–9215 (2003).
14. H. Kano, and H. Hamaguchi, "Vibrationally resonant imaging of a single living cell by supercontinuum-based multiplex coherent anti-Stokes Raman scattering microspectroscopy," *Opt. Express* **13**(4), 1322–1327 (2005).
15. T. Hellerer, A. M. K. Enejder, and A. Zumbuscha, "Spectral focusing: High spectral resolution spectroscopy with broad-bandwidth laser pulse," *Appl. Phys. Lett.* **85**(1), 25–27 (2004).
16. J. P. Ogilvie, E. Beaurepaire, A. Alexandrou, and M. Joffre, "Fourier-transform coherent anti-Stokes Raman scattering microscopy," *Opt. Lett.* **31**(4), 480–482 (2006).
17. K. Isobe, A. Suda, M. Tanaka, F. Kannari, H. Kawano, H. Mizuno, A. Miyawaki, and K. Midorikawa, "Fourier transform spectroscopy combined with 5-fs broadband pulse for multispectral nonlinear microscopy," *Phys. Rev. A* **77**, 063832/1–13 (2008).
18. K. Naganuma, K. Mogi, and H. Yamada, "General method for ultrashort light pulse chirp measurement," *IEEE J. Quantum Electron.* **25**(6), 1225–1233 (1989).
19. K. Isobe, A. Suda, M. Tanaka, F. Kannari, H. Kawano, H. Mizuno, A. Miyawaki, and K. Midorikawa, "Multifarious control of two-photon excitation of multiple fluorophores achieved by phase modulation of ultra-broadband laser pulses," submitted.
20. M. Greve, B. Bodermann, H. R. Telle, P. Baum, and E. Riedle, "High-contrast chemical imaging with gated heterodyne coherent anti-Stokes Raman scattering microscopy," *Appl. Phys. B* **81**(7), 875–879 (2005).

1. Introduction

Coherent anti-Stokes Raman scattering (CARS) is a nonlinear Raman process in which pulsed light of at least two frequencies is mixed within a sample. By temporally and spatially overlapping the pump light at a frequency of ω_p and Stokes light at ω_s , CARS light at a frequency of $2\omega_p - \omega_s$ is produced. When the frequency difference ($\omega_p - \omega_s$) can be tuned to specific vibrational resonances within a sample, CARS microscopy provides intrinsic vibrational contrast [1,2]. Two synchronized narrowband pulsed lasers are often employed as an excitation light source [3]. The relative spatial overlap and/or timing jitter between the pump and Stokes pulses has been the limiting factor, severely restricting the sensitivity or the signal-to-noise ratio. This problem can be solved by single-pulse CARS microscopy where the CARS process is induced by a single broadband pulse with pump and Stokes frequency components. However, single-pulse CARS microscopy has two inherent difficulties. One difficulty is that the resonant CARS signal is accompanied by significant nonresonant CARS signals from the electronic contribution [4]. Another difficulty results from the simultaneous excitation of various Raman modes with energies within the pulse bandwidth. As a result the spectral resolution is limited by the pulse bandwidth. Thus, it is necessary to suppress both the nonresonant signals and the resonant signals from nontarget Raman modes or to extract only the target signal of the single Raman mode at Ω_R . The nonresonant signals can be suppressed by various detection techniques including epi-detection [4,5], interferometric detection [6,7], polarization detection [8,9], or time-delayed detection [10]. However, in these techniques, the resonant signals from nontarget Raman modes cannot be reduced. Silberberg's group has reported other techniques that use the spectral phase modulation of a broadband pulse [11–13]. One is the selective excitation of a vibrational mode with wave number Ω_R by a periodic modulation of the spectral phase [11,13]. In the periodic modulation, the nonresonant signal decreases, while the resonant signals of the Raman mode with wave number $N\Omega_R$, where N is an integer, is also present. Another technique is single-pulse multiplex CARS spectroscopy where phase shifting of a narrow spectral band enables an effective narrow probing of the vibrational mode [12,13]. Even though the nonresonant CARS signal is not suppressed, the resonant signal of a single Raman mode can be extracted from analysis of the CARS spectrum [12–14]. The spectral analysis also provides multi-spectral images based on various Raman modes.

In this paper, we demonstrate two approaches to overcome the two difficulties in single-pulse CARS microscopy. The two types of microscopy can be achieved using the same setup and are complementary techniques. One approach is the novel spectral phase modulation for selective excitation of a single Raman mode without excitation of other Raman modes. This technique is similar to the spectral focusing technique based on two chirped excitation pulses to focus their bandwidth into a narrow spectral region [15]. The difference is that the spectral

focusing is realized not by using a pair of equally linear-chirped pulses from two synchronized lasers but by controlling the spectral phase of a single ultrabroadband pulse. Another approach is Fourier-transform CARS (FT-CARS) microspectroscopy where the CARS spectrum is obtained from the Fourier-transform of an interferometric autocorrelation (IAC) signal. FT-CARS microspectroscopy allows the suppression of the nonresonant signal and the measurement of a broadband CARS spectrum with high spectral resolution regardless of the pulse bandwidth [16,17]. The CARS spectrum is also used for choosing the excitation pulse for selective excitation CARS microscopy. Although FT-CARS microspectroscopy has been demonstrated [16], the practical applicability to biological samples has not yet been achieved. We apply FT-CARS microspectroscopy to imaging an unstained HeLa cell and obtain multi-spectral images from the CARS spectra. We also show that the difference between CARS spectra can be quantified by a normalized spectral correlation (NSC) technique, with which identification of specific organella can be achieved. Following this introduction, in Section 2, we show the principle of selective excitation of a single Raman mode. In Section 3, we propose a novel technique for measuring the difference-frequency (DF) spectrum of an excitation pulse, which indicates the characteristics of the selective excitation, without an infrared (IR) spectrometer. The IR spectrometer is used for directly measuring the difference-frequency generation (DFG). In Section 4, we report on experiments on selective excitation CARS microscopy and FT-CARS microspectroscopy. In Section 5, we summarize this paper.

2. Principle of selective excitation of a single vibrational mode

Here we describe how we create the spectral phase for selective excitation of a single vibrational mode in the CARS process induced by a single ultrabroadband pulse. In order to excite a single vibrational mode Ω_R , the spectral phase of a broadband pulse is controlled in the following manner. The quadratic phase $\phi''(\omega-\omega_0)^2/2$ is applied over the entire spectral region and then the linear phase $\phi''\Omega_R(\omega-\omega_{\max} + \Omega_R)$ is applied in the region where the frequency is smaller than $\omega_b = \omega_{\max}-\Omega_R$. Here, ϕ'' , ω , ω_{\max} and ω_0 are the group delay dispersion (GDD), the frequency of the pulse, the maximum frequency and the central frequency of the pulse. The phase function for selective excitation is described by

$$\varphi(\omega) = \begin{cases} \frac{\phi''}{2}(\omega - \omega_0)^2 + \phi''\Omega_R(\omega - \omega_b) & (\omega < \omega_b = \omega_{\max} - \Omega_R) \\ \frac{\phi''}{2}(\omega - \omega_0)^2 & (\omega \geq \omega_b). \end{cases} \quad (1)$$

The designed time-spectral distribution of the modulated pulse is shown in Fig. 1. As shown in Fig. 1, the frequency difference between ω_p and ω_s is constant at all times. Therefore, only a single vibrational motion is excited by focusing the DF spectrum into Ω_R . The bandwidth of the DF spectrum narrows with an increase in the GDD.

3. Principle of DF spectrum measurement without an IR spectrometer

To characterize the selective excitation of a single Raman mode, measurement of the DF spectrum of the excitation pulse is required. We propose a novel technique for measuring the DF spectrum without an IR spectrometer, which is used for directly measuring the DF pulse generated from a nonlinear crystal. This technique is based on an IAC measurement by nonresonant second-harmonic generation (SHG). By designing the pulsed electric field to be $E(t) = A(t)\exp(i\omega_0 t)$, the measured intensity of the IAC can be written as

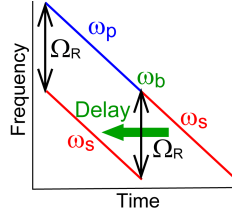


Fig. 1. Time-spectral distribution of excitation pulse for selective excitation of a single Raman mode.

$$\begin{aligned}
 I_{\text{SH}}(\tau) &\propto \int_{-\infty}^{\infty} \left| \{E(t) + E(t-\tau)\} \right|^2 dt \\
 &= 1 + 2G_2(\tau) + 4\text{Re}[F_1(\tau)\exp(i\omega_0\tau)] + \text{Re}[F_2(\tau)\exp(i2\omega_0\tau)],
 \end{aligned} \tag{2}$$

where τ is the relative delay between two pulses and where we define $G_2(\tau)$, $F_1(\tau)$ and $F_2(\tau)$ as [18]

$$G_2(\tau) = \int_{-\infty}^{\infty} |A(t)|^2 |A(t-\tau)|^2 dt, \tag{3}$$

$$F_1(\tau) = \int_{-\infty}^{\infty} \left\{ |A(t)|^2 + |A(t-\tau)|^2 \right\} A(t)A^*(t-\tau) dt, \tag{4}$$

$$F_2(\tau) = \int_{-\infty}^{\infty} A^2(t)A^{*2}(t-\tau) dt \tag{5}$$

Here, $A(t)$ is a slowly varying amplitude. The Fourier transform of $G_2(\tau)$ is expressed by

$$\text{FT}[G_2(\tau)] = \left| \int_{-\infty}^{\infty} \tilde{A}(\omega)\tilde{A}^*(\omega-\Omega) d\omega \right|^2. \tag{6}$$

Since Eq. (6) indicates the DF spectrum, we can acquire the DF spectrum from the Fourier-transform of the IAC signal.

4. Experimental

4.1 Experimental setup

A schematic of the experimental setup is shown in Fig. 2. As a broadband light source, we employed a Ti:sapphire laser operating at a repetition rate of 80 MHz. The laser spectrum ranged from 670 nm to 1150 nm. In order to compensate for second-order dispersion of all the optical components, the laser pulse was passed through a fused silica prism pair. A grating-pair-formed pulse shaper with a liquid-crystal spatial light modulator (SLM) (Cambridge Research & Instrumentation, Inc., LC-SLM-128) took on the task of compensating for the higher-order dispersion and additional shaping for the selective excitation by modulating the spectral phase of the ultrabroadband pulse [19]. At the SLM, the spectrum was limited to the region from 680 nm to 1020 nm to improve the spectral resolution of the spectral phase modulation. The spectral bandwidth of the output pulse from the SLM was 4800 cm^{-1} . The modulated pulse was sent into a Michelson interferometer. The output pulse was focused into the sample by an objective lens (OB) (Olympus Corporation, UPLSAPO40 \times , numerical aperture 0.9) whose chromatic and spherical aberrations were optimized for the spectral region from the visible region to the near-infrared region. The resultant signal was detected by a photomultiplier tube (PMT) (Hamamatsu Photonics, R4220) after excitation light was eliminated by a short-pass filter (SPF) (Semrock, FF01-680/SP-25). The sample was scanned by utilizing a three-axis piezoelectric transducer (PZT) stage. The dwell times per pixel in selective excitation CARS microscopy and in FT-CARS microspectroscopy were 200 μs and 410 ms, respectively. By measuring the signal intensity profile from a polystyrene bead with a

diameter of 350 nm, we determined the lateral point spread function with full width at half maximum (FWHM) of 416 nm, which was better than the Rayleigh diffraction limit. From this result, we found that chromatic aberration could be negligible. By scanning the delay stage in the interferometer, IAC signals were obtained. The maximum delay time was 533 fs. In selective excitation CARS microscopy, only one half of the output from the interferometer was employed as an excitation light source. The incident powers at the sample in selective excitation CARS microscopy and in FT-CARS microspectroscopy were 0.7 mW and 1.5 mW, respectively.

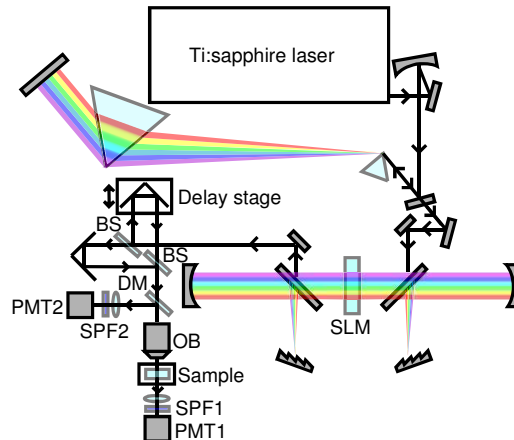


Fig. 2. Experimental setup. BS: beam splitter, OB: objective lens, DM: dichroic mirror, PMT1: photomultiplier tube for forward-detection, PMT2: photomultiplier tube for epi-detection, SPF: short-pass filter, SLM: spatial light modulator.

4.2 Selective excitation CARS microscopy

To confirm the spectral focusing, we measured the DF spectrum of the modulated pulse to selectively excite a single vibrational motion by the IAC technique. A 10- μm -thick β -barium borate (BBO) crystal was used. Figure 3(a) shows the GDD dependence of the DF spectrum. We found that the bandwidth of the DF spectrum narrowed with increasing GDD. It must be emphasized that the selective excitation allows a nearly 50-fold increase of the spectral resolution over the spectrum bandwidth of the excitation pulse. The achievable bandwidth of the DF spectrum was limited by the pixel number of the SLM because the maximum applied GDD was determined by the SLM pixel number. By increasing the pixel number, we could improve the bandwidth of the DF spectrum. Figure 3(b) shows the DF spectra obtained by using the modulated pulses to selectively excite different vibrational modes. From this result, we confirmed that arbitrary vibrational modes in the laser spectrum could be selectively excited.

We demonstrated the selective excitation of a single vibrational mode. The sample was acetone, sandwiched between a hole slide glass and a cover slip. The sample was scanned in the axial direction, where the excitation wave numbers were set to 2930 cm^{-1} and 3400 cm^{-1} . These were identified by CH stretching and nonresonant vibration, respectively. The red and green lines in Fig. 4 show the axial distributions of the CARS signals at 2930 cm^{-1} and 3400 cm^{-1} , respectively. The CARS signals were normalized against those obtained from the cover slip. Contrast ratios of 6.5:1 and 0.6:1 were obtained for acetone/glass and glass/acetone, respectively. It should be noted that the selective excitation of the CH stretching vibration at 2930 cm^{-1} was achieved by the use of the spectral phase modulation of a single ultrabroadband pulse with a spectral bandwidth of 4800 cm^{-1} .

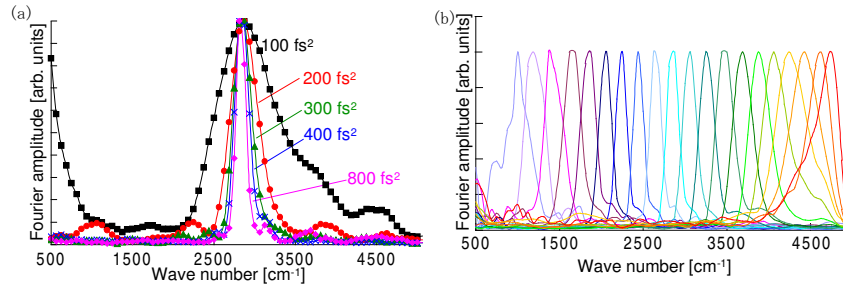


Fig. 3. (a) GDD dependence of the DF spectrum. (b) Focusing the DF spectrum into various narrow spectral regions.

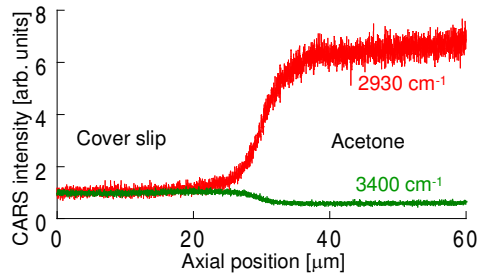


Fig. 4. Intensity cross sections of acetone, sandwiched between a hole-slide glass and a cover slip, by selective excitation at 2930 cm^{-1} (red) and 3400 cm^{-1} (green).

Next, we applied the selective excitation to vibrational imaging of an unstained HeLa cell. Figures 5(a), 5(b) and 5(c) show the CARS images at excitation wave numbers of 2930 cm^{-1} , 3200 cm^{-1} and 3400 cm^{-1} , respectively. To suppress the nonresonant CARS signals, these images were obtained with epi-detection. Figure 5(a) shows a much stronger signal for mitochondria, endoplasmic reticula and the nucleus, which are rich in C-H, while Figs. 5(b) and 5(c) illustrate CARS signals not only from mitochondria, endoplasmic reticulum and the nucleus but also from water and from the cover slip around cell. We found that CH vibrational imaging was successfully obtained at a wave number of 2930 cm^{-1} .

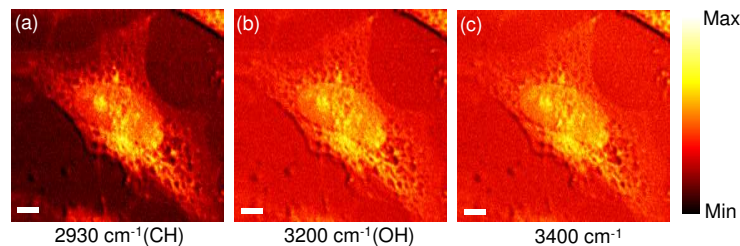


Fig. 5. CARS images of an unstained HeLa cell by selective excitation at 2930 cm^{-1} (a), 3200 cm^{-1} (b) and 3400 cm^{-1} (c). Scale bar is $6\text{ }\mu\text{m}$.

4.3 FT-CARS microspectroscopy

To obtain a point by point CARS spectrum, we adapted FT-CARS microspectroscopy. By measuring an IAC signal in a delay time range longer than the pulse duration, the nonresonant CARS signal was removed [16]. In FT-CARS microspectroscopy, the CARS signals were obtained with forward detection. For the excitation pulse, we employed a Fourier-transform-limited pulse with a pulse duration of 5.3 fs [16]. Figure 6(a) shows the Fourier spectrum of an IAC signal from acetone. We confirmed that the FT-CARS technique gave a CARS spectrum ranging from 1000 cm^{-1} to 5000 cm^{-1} that simultaneously did not include the

nonresonant CARS signal. From the inverse of the maximum delay time, we estimated the spectral resolution to be on the order of 60 cm^{-1} . Multi-spectral CARS images of a polystyrene bead in acetone were obtained by FT-CARS microspectroscopy. Figures 6(b), 6(c) and 6(d) show CARS images constructed from the integration in spectral bands of $0\text{-}100 \text{ cm}^{-1}$, $2800\text{-}2950 \text{ cm}^{-1}$, and $3000\text{-}3100 \text{ cm}^{-1}$, which indicates the nonresonant, the aliphatic CH vibration and the aromatic CH vibration, respectively. At the edge of the bead, the signal was clearly reduced. This phenomenon has been explained by destructive interference between the resonant CARS signal from beads and the nonresonant CARS signal from solvent. However, the nonresonant signals could be successfully suppressed as shown in Fig. 6(a). Thus, we concluded that the signal reduction was induced by reflection and scattering losses. From the result of time-gating CARS imaging for the efficient nonresonant CARS signal suppression, Greve *et al.* has also explained the signal reduction by reflection and scattering losses [20]. We found that with the spectral band of $2800\text{-}2950 \text{ cm}^{-1}$, both acetone and the polystyrene bead were visualized, while, with the spectral band of $3000\text{-}3100 \text{ cm}^{-1}$, only the polystyrene bead was imaged. It must be emphasized that the FT-CARS microspectroscopy provided multi-spectral CARS images with a Raman frequency difference of 100 cm^{-1} even though an excitation pulse with a spectral bandwidth of 4800 cm^{-1} was employed.

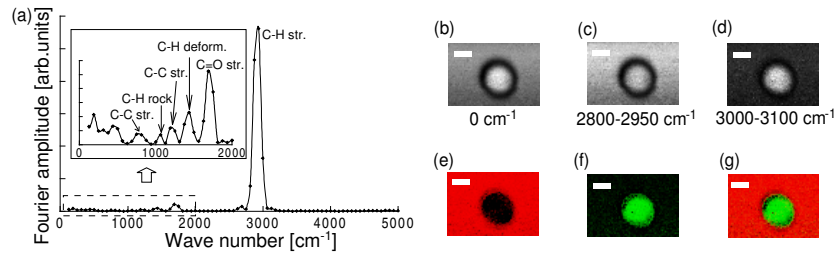


Fig. 6. (a) Fourier spectrum of CARS-IAC signal from acetone. (b-d) CARS images of a polystyrene bead constructed from the integration in spectral bands of $0\text{-}100 \text{ cm}^{-1}$ (b), $2800\text{-}2950 \text{ cm}^{-1}$ (c), and $3000\text{-}3100 \text{ cm}^{-1}$ (d). (e-f) CARS images of a polystyrene bead in acetone reconstructed after the NSC process using the CARS spectrum from acetone (e) and the polystyrene bead (f). (g) Combined image of the two CARS images of (e) and (f). Scale bar is $2 \mu\text{m}$.

To realize images from the CARS spectra, we define C_{SP} as the value of the normalized spectral correlation (NSC) given by

$$C_{\text{SP}} = \frac{\frac{1}{n} \sum_{i=0}^n S_s(\lambda_i) S_r(\lambda_i)}{\sqrt{\frac{1}{n} \sum_{i=0}^n S_s^2(\lambda_i)} \sqrt{\frac{1}{n} \sum_{i=0}^n S_r^2(\lambda_i)}}, \quad (7)$$

where $S_s(\lambda_i)$ and $S_r(\lambda_i)$ represent the CARS spectra from the sample and the reference, respectively. We used the spectral range from 1000 to 3500 cm^{-1} . The value of NSC provides a quantitative comparison between the sample and reference spectra regardless of the signal intensity. Although information about the signal intensity is lost due to the use of the normalized CARS spectrum, NSC analysis allows us to identify regions of specific molecules by the use of the similarity of the CARS spectrum. Figures 6(e) and 6(f) show the images reconstructed after NSC processes using the CARS spectrum from acetone and that from the polystyrene bead as the reference spectrum, respectively. Figure 6(g) illustrates a combined image of the two images shown in Figs. 6(e) and 6(f). The regions of acetone and the polystyrene bead are clearly divided. It should be noted that the acetone and the polystyrene bead were identified by features in the CARS spectra.

Finally, we demonstrate the practical applicability to biological samples of FT-CARS microspectroscopy. For the sample, we used an unstained HeLa cell. Figures 7(a) and 7(b) show CARS images constructed from integration in the spectral bands of 2800-2900 cm^{-1} and 2900-3000 cm^{-1} . Strong signals from mitochondria or endoplasmic reticula are shown in both Figs. 7(a) and 7(b), while enhanced signals from the nucleus are illustrated only in Fig. 7(b). To visualize this difference, we employed the NSC process. Figure 7(c) shows a combined image of three images reconstructed after NSC processes using the CARS spectra from mitochondrion or endoplasmic reticulum (Blue), the nucleus (Green) and water around the cell (Red) as the reference spectrum. Although the image contrast of Fig. 7(c) looks saturated because of the loss of information about the signal intensity, We successfully achieved identification of the specific organella.

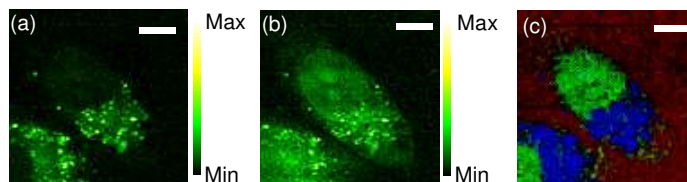


Fig. 7. (a, b) CARS images of an unstained HeLa cell constructed from integration in the spectral bands of 2800-2900 cm^{-1} (a), and 2900-3000 cm^{-1} (b). (c) Combined image of three CARS images of an unstained HeLa cell reconstructed after the NSC process using the CARS spectrum from mitochondria or endoplasmic reticulum (blue), the nucleus (blue) and water (red). Scale bar is 8 μm .

5. Conclusion

In conclusion, we demonstrated two types of single-pulse CARS microscopy employing a single ultrabroadband laser pulse with a spectral bandwidth of 4800 cm^{-1} . One type is selective excitation CARS microscopy, which is based on the use of a chirped excitation pulse to focus its DF spectrum into a narrow Raman band. The spectral focusing, which was achieved by spectral phase modulation of the single ultrabroadband pulse, was confirmed by a SHG-IAC technique without an IR spectrometer. By imaging the interface between acetone and a cover slip, we demonstrated selective excitation of the CH stretching vibration at 2930 cm^{-1} . From the selective excitation at 2930 cm^{-1} , we obtained the CARS image of mitochondria and the nucleus in an unstained HeLa cell. The other type of microscopy is FT-CARS microspectroscopy employing a 5-fs pulse. We demonstrated that with FT-CARS microspectroscopy the nonresonant CARS signal can be suppressed, a spectral resolution of 60 cm^{-1} can be achieved and a CARS spectrum with a bandwidth of 4000 cm^{-1} can be obtained in a single measurement. Multi-spectral CARS images of a polystyrene bead in acetone were obtained by FT-CARS microspectroscopy. By a point by point NSC process of a CARS spectrum, acetone and a polystyrene bead were successfully discriminated. We also showed that FT-CARS microspectroscopy using the NSC process allowed the identification of mitochondria and the nucleus in an unstained HeLa cell. The two types of single-pulse CARS microscopy can be realized using the same setup. The excitation pulse for selective excitation CARS microscopy can be chosen from the CARS spectrum, which is acquired by FT-CARS microspectroscopy, at a specific position in the sample. Switching between selective excitation CARS microscopy and FT-CARS microspectroscopy as the situation demands is a powerful technique for identifying molecules and mapping specific molecules in a complementary style.

Acknowledgments

We thank Prof. Dr. T. Kitajima, Prof. Dr. Y. Itoh and Prof. Dr. I. Ishikawa in RIKEN for providing the biological sample. This research was supported by the Special Postdoctoral Researchers Program of RIKEN.